A&A 609, A69 (2018)
DOI: 10.1051/0004-6361/201629920

Astronomy & Astrophysics

Numerical modeling of the 1840s major eruption of η Carinae as an explosion

Ricardo F. González

Instituto de Radioastronomía y Astrofísica, Universidad Nacional Autónoma de México, A.P. 3-72 (Xangari) 58089 Morelia, Michoacán, México
e-mail: rf.gonzalez@crya.unam.mx

Received 18 October 2016 / Accepted 14 November 2017

ABSTRACT

In this paper, new two-dimensional hydrodynamical simulations of η Car's nebulae are performed. In the 1840s, the massive star η Car suffered a major eruption that resulted in the formation of a bipolar structure, which is commonly known as the large Homunculus. During this event, η Car expelled into the circumstellar material a total mass of $\sim$10 $M_\odot$ and released a total energy of $E_k \sim 10^{50}$ erg over a very short time ($\leq$5 yr). These kinds of explosive events are frequently called supernova impostors due to their resemblance to a type II supernova, but the stars survive the explosion. In the case of η Car, a brief explosion scenario provides a potential explanation for the behavior of the historical light curve of η Car a few years ($\sim$10 yr) after the nineteenth century outburst. Here, such an alternative scenario of an explosion is assumed (instead of a super-Eddington wind) in order to investigate whether an explosive event is also able to explain the shape and kinematics of the large Homunculus. I show that the numerical simulations presented here indeed resemble some of the observed features of the nebula, such as the present-day double-shell structure of the Homunculus, with a thin outer dense shell and a thicker inner layer, as well as thermal instabilities (Rayleigh-Taylor and Kelvin-Helmholtz) along the dense shell that may lead to the current mottled appearance of the large Homunculus. Nonetheless, the explosion model for the 1840s major eruption of η Car is not able to account for the estimated age of the large Homunculus.

Key words. stars: individual: η Carinae – stars: winds, outflows – hydrodynamics – shock waves

1. Introduction

The star η Car is an evolved star of $\sim$90 $M_\odot$ orbited in a highly eccentric orbit of $\sim$0.9 (Damineli et al. 1997) by a main sequence star of $\sim$30 $M_\odot$ (e.g., Portegies Zwart & van den Heuvel 2016). Located at 2.3 kpc, the primary star η Car has undergone violent mass-loss episodes that may be related to its strict 5.54 yr periodicity in its light curve (Damineli 1996). In the decade of the 1840s (around the year 1843), one of these eruptive events occurred, which is called the major eruption, when the star launched large amounts of mass into the surroundings, and its historical light curve showed a drastic increase in its visual magnitude (Humphreys et al. 1999). From this eruption, the observed bipolar nebula (commonly known as the large Homunculus) was formed, which has a current angular size of $\sim\pm9''$ (that corresponds to a physical size of $\pm3.2 \times 10^{17}$ cm) and expands at a speed of $\sim$650 km s^{-1} along its major axis (see Smith 2006). In other work, Smith et al. (2003) estimated from thermal infrared images of η Car a total mass $\geq$12.5 $M_\odot$ contained in the Homunculus nebula. Most of this mass ($\sim$10 $M_\odot$) was expelled during the major eruption and resides in a cool molecular layer that traces the outer walls of the Homunculus, whereas 10 percent of the mass resides in a thicker shell of atomic gas that resides immediately interior to the polar lobes.

In addition, Smith (2006) presented near-infrared high-resolution spectra of the three-dimensional structure of the large Homunculus around η Car, which confirm the double-shell structure inferred previously by Smith et al. (2003). The new near-infrared spectra obtained by this author resolved the nebula into a very thin outer shell detected in H_2 and a thicker inner shell seen in [Fe II] that partially fills the interior of the polar lobes. Based on the H_2 spectra that show how thin the outer molecular layer is, this author concluded that the mass-loss phase during the eruptive event lasted only a few years ($\sim$5 yr or less), and suggested that the major eruption of η Car in the nineteenth century can be considered as an explosion instead of a stellar wind.

In the year of 1890, the historical light curve of η Car shows evidence of a minor eruptive event from which an internal nebula, embedded within the large Homunculus, was formed. Ishibashi et al. (2003) reported spectroscopic mapping obtained with the *Hubble* Space Telescope (HST) using the Space Telescope Imaging Spectrograph (STIS) of η Car's nebulae that detects emission, also with bipolar geometry, extending from $-2''$ to $+2''$ across the star. The estimated total mass expelled by the star of $\sim$0.1–0.2 $M_\odot$ and the total kinetic energy released of $\sim10^{46.9}$ erg in the 1890 event (see Smith 2005) are orders of magnitude less than the corresponding values during the major eruption, which indicates that the physical processes involved in both eruptions were very different.

More recently, Smith (2013) proposed to model the 1840s major eruption of η Car as an explosion (rather than a "super-Eddington" wind) that collides with a strong pre-eruptive wind. This explosive event of the mid-nineteenth century suffered by η Car was analogous to a type IIn supernova explosion, but with lower energy released to the circumstellar medium, and hence, is often referred to as a supernova impostor. According to this author, the collision between the fast material and the surrounding circumstellar matter (CSM) provides a close match to the high-luminosity stage observed in the historical light curve during the 10–15 yr after the eruption. In addition, different physical

Table 1. Models of the η Car's explosion: parameters of the colliding outflows.

Run	Outflow phase	λ	v_1 [km s^{-1}]	v_2 [km s^{-1}]	Δt [yr]	$\dot{m}$ [$M_\odot$ yr^{-1}]
A	Standard wind	2.4	250	14	507	1.0×10^{-3}
	Pre-eruptive wind	2.4	250	14	30	3.3×10^{-1}
	Explosion	1.9	800	100	1	1.0×10^{1}
	Post-outburst wind	1.9	500	14	49	1.0×10^{-3}
	Minor eruption	1.9	200	10	10	1.0×10^{-2}
	Post-eruption wind	1.9	500	300	–	1.0×10^{-3}
B	Standard wind	1.9	500	30	254	1.0×10^{-3}
	Pre-eruptive wind	2.4	250	14	30	3.3×10^{-1}
	Explosion	1.9	800	100	1	1.0×10^{1}
	Post-outburst wind	1.9	500	30	49	1.0×10^{-3}
	Minor eruption	1.9	200	10	10	1.0×10^{-2}
	Post-eruption wind	1.9	500	300	–	1.0×10^{-3}
C	Standard wind	1.9	500	14	254	1.0×10^{-3}
	Pre-eruptive wind	2.4	200	10	30	3.3×10^{-1}
	Explosion	1.9	750	100	1	1.0×10^{1}
	Post-outburst wind	1.9	500	14	49	1.0×10^{-3}
	Minor eruption	1.9	200	10	10	1.0×10^{-2}
	Post-eruption wind	1.9	500	300	–	1.0×10^{-3}
D	Standard wind	2.4	300	14	423	1.0×10^{-3}
	Pre-eruptive wind	2.4	200	10	40	2.5×10^{-1}
	Explosion	1.9	750	100	2.5	4.0×10^{0}
	Post-outburst wind	1.9	500	14	47.5	1.0×10^{-3}
	Minor eruption	1.9	200	10	10	1.0×10^{-2}
	Post-eruption wind	1.9	500	300	–	1.0×10^{-3}

Notes. The 1890's minor eruption and post-eruption wind conditions are taken from González et al. (2010).

properties of the large Homunculus are addressed in that work; in particular, the model accounts for the double-shell structure of the nebula.

Different models have been proposed to study the formation and evolution of η Car's bipolar nebula (e.g., Maeder & Desjacques 2001; Dwarkadas & Owocki 2002; Frank et al. 1995, 1998; Dwarkadas & Balick 1998; Langerv et al. 1999; Soker 2001, 2007; Steffen et al. 2014). Previously, in González et al. (2004a,b) and González et al. (2010), we modeled η Car's major eruption assuming an interacting non-spherical multiphase wind scenario, in which the eruptions are considered as transient conditions of η Car's stellar wind. In our previous models, the large Homunculus is produced by the interaction of the 1840s major eruption with the underlying stellar wind.

Here, I present new numerical simulations of η Car's nebula adopting the alternative scenario (proposed by Smith et al. 2013) of an explosive event during the major eruption in the 1840s. I have modified our previous colliding-wind models, and explored through numerical simulations whether this scenario of a brief explosion is able to account for not only the light curve a few years after the eruption but also the shape and kinematics of η Car's Homunculus. The inner mechanism that triggered the explosion at scales of the central source of η Car is not addressed in this work but, as stressed in our previous models, it may be connected with a binary star system. González et al (2010) studied the formation and dynamical evolution of the outflows and shocks associated with the large Homunculus at much larger scales ($>10^{17}$ cm) than the physical size of the binary orbit (4.5×10^{13} cm at periastro, and 2.1×10^{14} cm at apoastro), but the binary origin of the eruption is not ruled out.

The plan of the paper is as follows. In Sect. 2, the numerical method and initial physical conditions are described. The numerical simulations are presented in Sect. 3. Finally, in Sect. 4, I discuss the implications of the results and draw some conclusions.

2. Numerical method and initial physical conditions

I have performed new numerical simulations of the 1840s major eruption of the massive star η Car, using a two-dimensional hydrodynamic version of the Yguazú-A adaptive grid code developed by Raga et al. (2000). This code integrates the hydrodynamic equations explicitly accounting for the radiative cooling for the atomic and ionic species HI, HII, HeI, HeII, HeIII, CII, CIII, CIV, OI, OII, and OIII. The flux-vector splitting algorithm of Van Leer (1982) is employed. The numerical simulations were carried out on a five-level binary adaptive grid with a maximum resolution along each axis- of 3.9×10^{14}cm. The computational domain extends over (4×10^{17} cm) $\times$ (4×10^{17} cm), corresponding to 1024×1024 grid points at the highest resolution level. At first, the computational domain is filled by a homogeneous ambient medium with a density of 10^{-3} cm^{-3} and a temperature of 10^2 K.

In Table 1, different models (Runs A–D) performed for the η Car's explosion are listed. In these numerical simulations,

slight variations in the flow parameters of the standard wind, pre-eruptive wind, and post-ouburst wind, as well as the 1840s explosion, are assumed. In all runs, the adopted parameters of the 1890s minor eruption and the wind blown afterwards are taken from González et al. (2010). In the table, I list the constant λ (that is related to the degree of asymmetry of the outflow) the velocities v_1 and v_2 related to the polar and equatorial directions, respectively (see below), the duration Δt of each outflow phase, and the corresponding mass-loss rate $\dot{m}$.

In contrast to our previous simulations of colliding winds (see Sect. 1), the physical parameters adopted here for the pre-eruptive wind and the major eruption are consistent with the CSM-interaction model proposed by Smith (2013). This author assumes two phases in this model, a strong wind of short duration (30 yr) followed by a brief explosion (1−5 yr). In both phases, 10 $M_\odot$ are ejected, and hence, the total mass involved in the interaction is 20 $M_\odot$. Assuming these parameters, the CSM interaction model presented by Smith (2013) provided a good fit to the observed shape and magnitude of η Car's light curve for 10 yr after the eruption. Consequently, this author pointed out that the 1840s major eruption can be considered as a scale-down type II supernova, since the total energy released during the eruptive event ($E \simeq 10^{50}$ erg) was approximately ten times lower than the energy of a normal supernova explosion. In Runs A–D, this explosion scenario is explored in order to investigate the impact on the shape and kinematics of the large Homunculus.

I have supposed for the different wind phases the latitude-dependent injection velocity and density proposed by González et al. (2010), that is,

$$v = v_1\, F(\theta), \tag{1}$$

and

$$n = n_0 \left(\frac{r_0}{r}\right)^2 \frac{1}{F(\theta)}, \tag{2}$$

respectively, where $r_0 = 10^{16}$ cm is the injection radius, and $F(\theta) = [(v_2/v_1) + e^{2z}]/[1 + e^{2z}]$ being $z = \lambda \cos(2\theta)$ a parameter that controls the shape of the Homunculus, λ is a constant, and θ is the polar angle. The velocity v_1 is related to the expansion speed v_P in the polar direction, while the velocity v_2 is related to the corresponding value v_E at equator. From Eqs. (1) and (2), it follows that a constant mass-loss rate per unit solid angle is assumed. González et al. (2010) showed that a theoretical curve with $\lambda = 1.9$, $v_1 = 670$ km s^{-1} , and $v_2 = 100$ km s^{-1} represents the best fit to the observed expansion speed at different latitudes of η Car's Homunculus (see, Smith 2006).

Initially, a standard wind is assumed, which sweeps up a homogeneous medium until the computational domain (along the y-axis) is filled. Later, a pre-eruptive wind is expelled for a few decades before η Car's explosion. In the numerical simulations, the duration and physical properties of both the pre-eruptive wind and the explosion are consistent with those proposed by Smith (2013).

Afterwards, a post-outburst wind (with similar conditions to the present-day stellar wind) is ejected until the minor eruption occurs. In all runs, the physical parameters of the second eruptive event and the posterior wind are taken from González et al. (2010), where we have already investigated the shape and kinematics of the little Homunculus (which was produced at the end of the minor eruption) and also the formation of high-velocity outflowing features at the equator (see, also, González et al. 2004a,b). The study of the internal nebula is not an issue of the current work. According to the CSM-interaction model described above, the explosion dominates the momentum flux and must determine the degree of asymmetry of the large Homunculus. In these simulations, the total mass contained inside the Homunculus is ≃20 $M_\odot$, with 10 $M_\odot$ ejected by the star during the pre-eruptive wind and 10 $M_\odot$ expelled in the explosion.

3. Numerical simulations

In this section, new results of gas dynamic simulations of η Car's nebula are presented. In contrast with our previous models (González et al. 2010), the 1840s eruptive event of the star is modeled as a brief explosion rather than a strong stellar wind. The aim of these new numerical simulations is to explore whether the CSM-interaction model developed by Smith (2013) to match the light curve of η Car one decade after the eruption can also account for the observed physical properties of the large Homunculus. It is shown that different results are predicted among the models.

Figure 1 depicts the results obtained from Run A of η Car's explosion. For this model, I employ the physical parameters adopted by González et al. (2010) for the standard wind and post-outburst wind, whereas the values for the pre-eruptive wind and the explosion are consistent with the CSM-interaction model. The log-scale maps of the density distribution of η Car's Homunculus at four different times of its dynamical evolution (10, 45, 80, and 120 yr after the explosion) are presented. The figure shows that the Homunculus nebula is formed from the interaction of the explosion with the pre-eruptive wind. Once the explosion occurs, (at $t \simeq 0$), a two-shock wave structure is formed, which accumulates material of both outflow phases. As we showed in our previous works, the assumed latitude-dependent flow parameters at injection are able to account for the bipolar shape of η Car's Homunculus as it propagates outward. The inward shock engulfs the fast and massive flow expelled during the explosion, while the outward shock sweeps the gas expelled during the pre-outburst wind. In this stage of evolution, the layer moves along the symmetry axis with constant velocity (≃640 km s^{-1}), which is an intermediate value between both outflow speeds (see Table 1). A few years (≃5.24 yr) after the explosion, all the fast material has entered the inward shock (in the polar direction), and the shocked layer is decelerated by the slower pre-outburst wind until it is completely incorporated into the forward shock (at $t \simeq 19.64$ yr), when the interaction ends up. Later, the forward shock sweeps up a slighter wind located ahead, while the inward shock propagates through a rarefied zone that resulted from the velocity drop of η Car's wind after the explosion. It is remarkable that this numerical simulation predicts that the large Homunculus reaches the current physical extension of the nebula (3.2×10^{17} cm) along the symmetry axis at $t = 120$ yr after the major eruption, long before the estimated age of the Homunculus nebula (≃174 yr). Furthermore, a polar velocity of the shell of ≃800 km s^{-1} is obtained, which is higher than the observed expansion speed of ≃650 km s^{-1} at high latitudes of the Homunculus (see, for instance, Smith 2006). Nevertheless, it is noteworthy that the computed density map, assuming a brief explosion scenario for the major eruption of η Car, depicts a morphology of the nebula that indeed resembles the double-shell structure of the Homunculus reported by this author, who detected a thin outer shell of H_2 and a thicker inner skin of [Fe II] that partially fills the interior of the lobes.

In order to investigate whether this explosion scenario is able to explain not only the light curve ∼10 yr after the 1840s η Car eruption, but also the present-day physical size and kinematics of

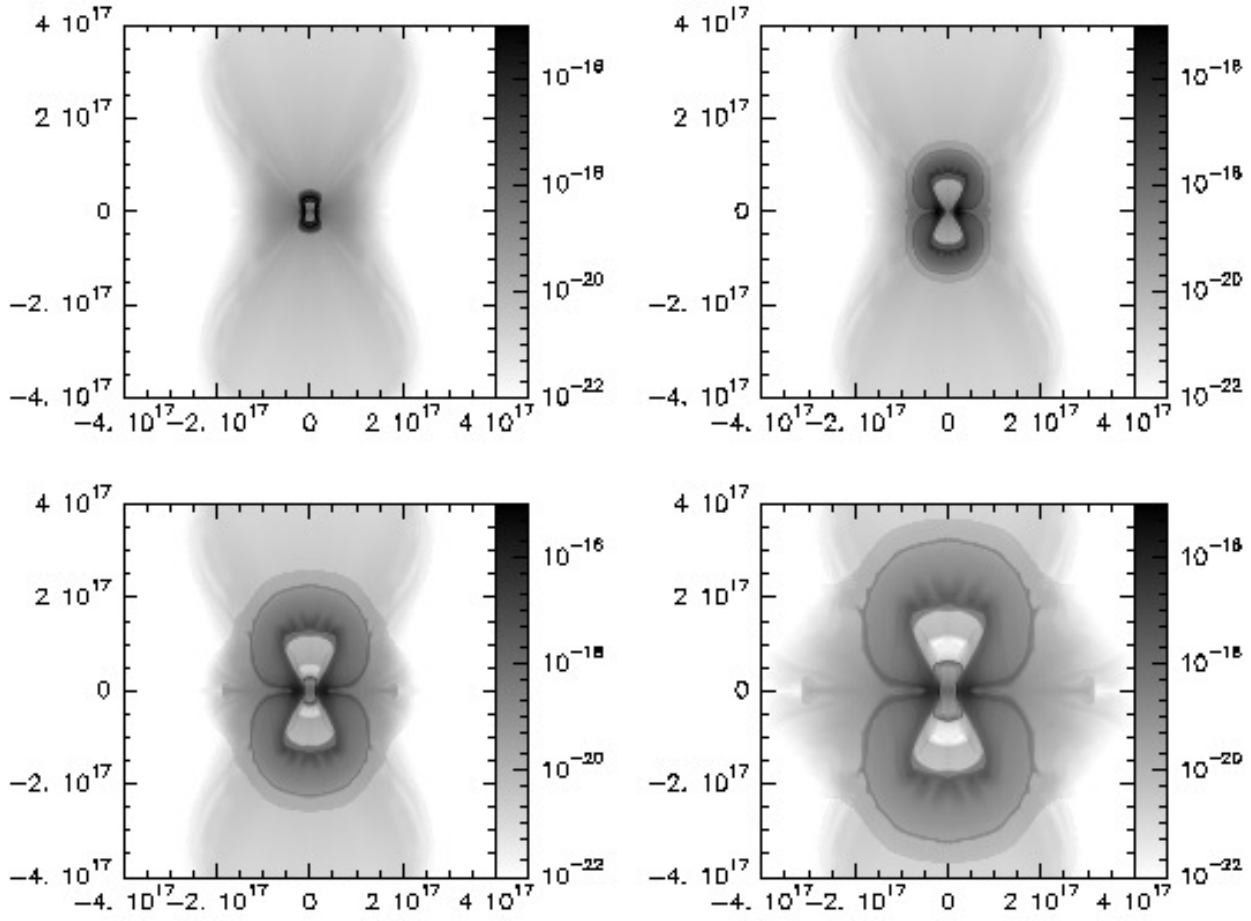

Fig. 1. Log-scale density stratification of η Car's nebulae for Run A. The panels correspond to four different times of integration after the explosion in the 1840s: t = 10 yr (*top left*); t = 45 yr (*top right*); t = 80 yr (*bottom left*); and t = 120 yr (*bottom right*). The bars at the right side of the plots are in units of g cm^{-3} and the computational domain axes are in units of cm. The physical description of the figure is given in the text.

the large Homunculus, I have carried out other numerical models of this eruptive event (Runs B−D). In these simulations, the injection parameters of the different outflow phases of η Car have been modified in order to explore the impact on the predicted properties of the nebula. The results of these numerical experiments are presented in Fig. 2.

In Run B, I considered distinct ejection velocities and latitude-dependent behavior for both the standard wind and post-outburst wind. Besides, the mass-loss rates during these outflow phases are the same as those adopted in Run A. In addition, the parameters of the colliding pre-eruptive wind and explosion have not been changed (see Table 1). It is worth mentioning that in Run B, the expansion velocity (at the poles) of the standard wind is more similar to the normal speed (≃600−1000 km s^{-1}) of η Car's stellar wind (see, for instance, Smith et al. 2003). At the time depicted in Fig. 2 (top-right), t = 104 yr after the explosion, the dense shell has already reached the current size (along the symmetry axis) of the Homunculus, which suggests that the interaction of the leading shock with the rarefied zone (between the standard wind and the pre-eruptive wind) causes the acceleration of the dense shell to higher speeds (≃890 km s^{-1}). Consequently, this model predicts a younger age of η Car's Homunculus than that computed from Run A.

In Run C, the outflow velocities of the pre-eruptive wind and the explosion have been modified. For both outflow phases, lower speeds are adopted. Figure 2 (bottom-left) shows the numerical simulation at time t = 103 yr after the explosion, when the dense shell has the present-day physical size of the large Homunculus. In addition, at this time the shell has an expansion speed of ≃930 km s^{-1} in the polar direction. These values of the age and velocity of the nebula are very similar to those obtained in Run B; nevertheless, Run C shows more clearly the thermal instabilities produced at the contact discontinuity.

In addition, Run D explores the impact of a longer duration of both the pre-eruptive wind and the explosion on the shape and kinematics of η Car's nebula. In this model, it is assumed that the outburst lasted 2.5 yr with a mass-loss rate of 4 $M_\odot$ yr^{-1}, while the pre-outburst wind is expelled during 40 yr with 0.25 $M_\odot$ yr^{-1}. Adopting these outflow parameters, the total mass ejected is 20 $M_\odot$, as the other runs assume. In Fig. 2 (bottom-right), the results of this run at time t = 121 yr after the major eruption are presented, when the polar lobes have reached the current size of the Homunculus. Therefore, this model, which assumes a longer CSM interaction, is also unable to explain the dynamical evolution of η Car's nebula.

On the other hand, Fig. 3 presents the pressure (top-left), temperature (top-right), density (bottom-left), and velocity field map superposed to the density map (bottom-right) for Run A, at time t = 120 yr since the great eruption. The simulation shows a dense layer at the contact discontinuity, which is located at a position $r \simeq 3.2 \times 10^{17}$ cm in the polar direction at this time. Besides, the double-shell structure of the Homunculus nebula can be seen, with an outer thin dense layer and an inner thicker shell behind. It is worth mentioning that at this time, the leading shock

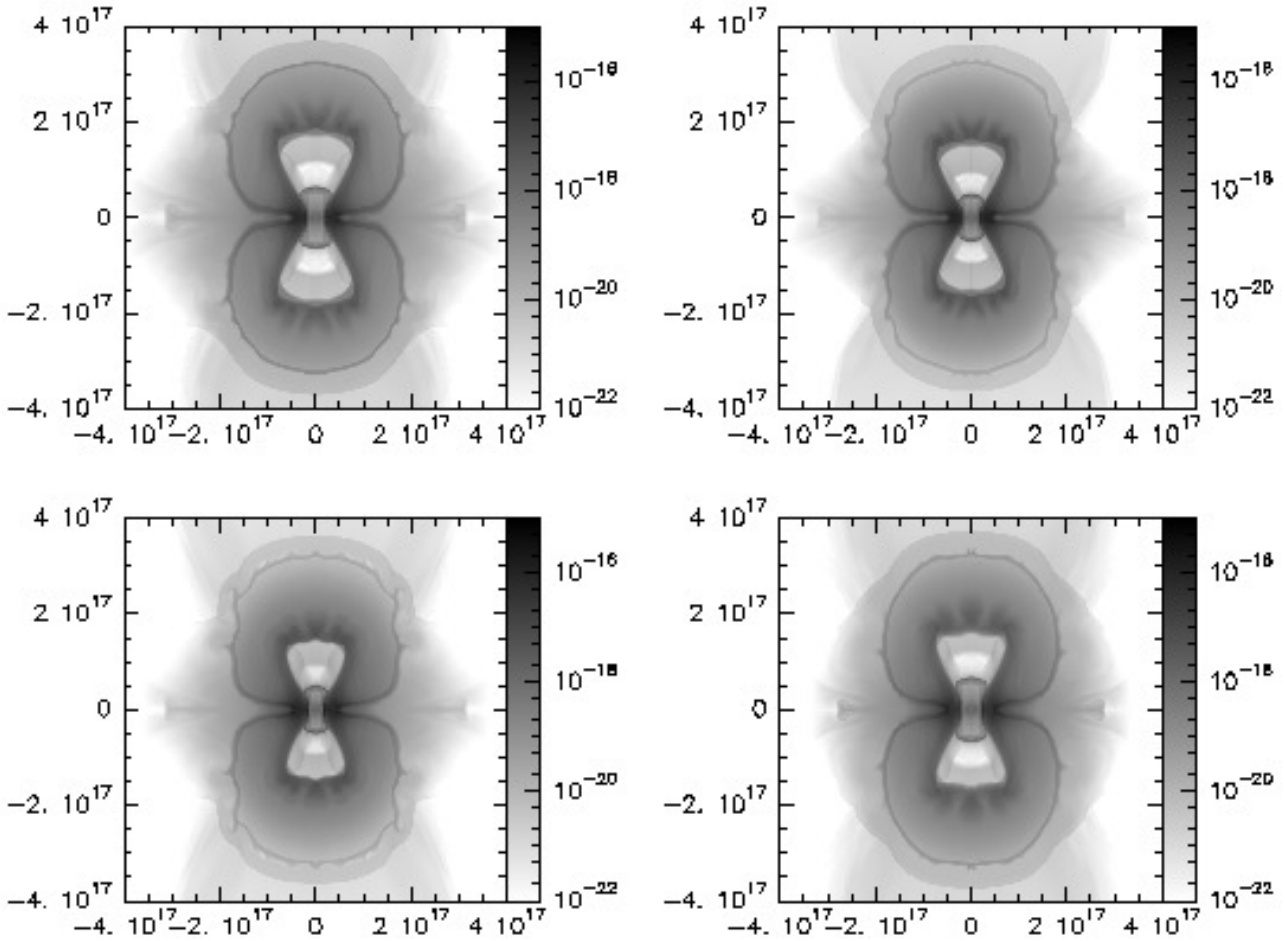

Fig. 2. Predicted density maps of η Car's nebula for Run A at a time t = 120 yr (*top left*), for Run B at t = 104 yr (*top right*), for Run C at t = 103 yr (*bottom left*), and for Run D at t = 121 yr (*bottom right*) after 1840s major eruption. The vertical bars at the right side of the plots depict the logarithmic grayscale of the density in g cm^{-3}, and the computational domain axes are labeled in cm. A detailed description of the figure is presented in the text.

(located at $\simeq 3.7 \times 10^{17}$ cm) is sweeping the standard wind, while the reverse shock (located at $\simeq 1.8 \times 10^{17}$ cm) is still engulfing the post-outburst wind. Consequently, the shock conditions in both shock fronts are completely different at this time to those given during the CSM interaction, when the explosion collides with the pre-outburst wind. A final remark is that the kinematic component of the thick inner skin of [Fe II] detected at 500 km s^{-1} by Smith (2006), which shows the presence of a low-emission cavity between both Homunculi, is consistent with the expansion velocity of the inner shell predicted by this numerical simulation. A speed is computed that increases (along the polar axis) from $\simeq$450 km s^{-1} just behind the inward shock to $\simeq$800 km s^{-1} at the contact discontinuity. In addition, the figure shows the presence of a rarefied zone between the Homunculi, from $r \simeq 0.7 \times 10^{17}$ to 1.2×10^{17} cm along the symmetry axis, which results from the velocity drop during the minor eruption.

Furthermore, as proposed by Smith (2013), who pointed out that the observed present-day mottled appearance of the large Homunculus (see also, Morse et al. 1998) may result from Rayleigh-Taylor or Vishniac instabilities at the cold dense shell with efficient radiative cooling (see, also, van Marle et al. 2010), the numerical simulations presented here show the presence of thermal instabilities (Rayleigh-Taylor and Kelvin-Helmholtz) along the dense shell. These instabilities are more noticeable in Run B and Run C, which assume a similar present-day expansion velocity of the standard wind. Furthermore, Richtmyer-Meshkov instabilities can also be seen just behind the inner boundary of the thicker shell, which arise from the interaction of the reverse shock with the interface between the dense gas expelled during the explosion and the lower density medium located below, which yields when the eruptive event finishes (see, for instance, Brouillette 2002).

4. Discussion and conclusions

In this work, new two-dimensional high-resolution hydrodynamical simulations of the 1840s major eruption of η Car were carried out. These simulations differ from our previous numerical models (González et al. 2004a,b; 2010), since this eruptive event is modeled here as an explosion rather than a super-Eddington wind. The CSM interaction model proposed by Smith (2013) for explaining the light curve of the star approximately ten years after the eruption, is adopted. On the other hand, I have borrowed from our numerical models of interacting winds (González et al. 2010) the non-spherical parameters of the colliding outflows for the 1890s η Car minor eruption.

Different numerical experiments have been developed, which assume distinct parameters for η Car's mass-loss phases (before, during, and after the explosion). These new numerical simulations indeed represent a potential explanation for the observed current morphology of the large Homunculus. In particular, they can account for the double-shell structure of

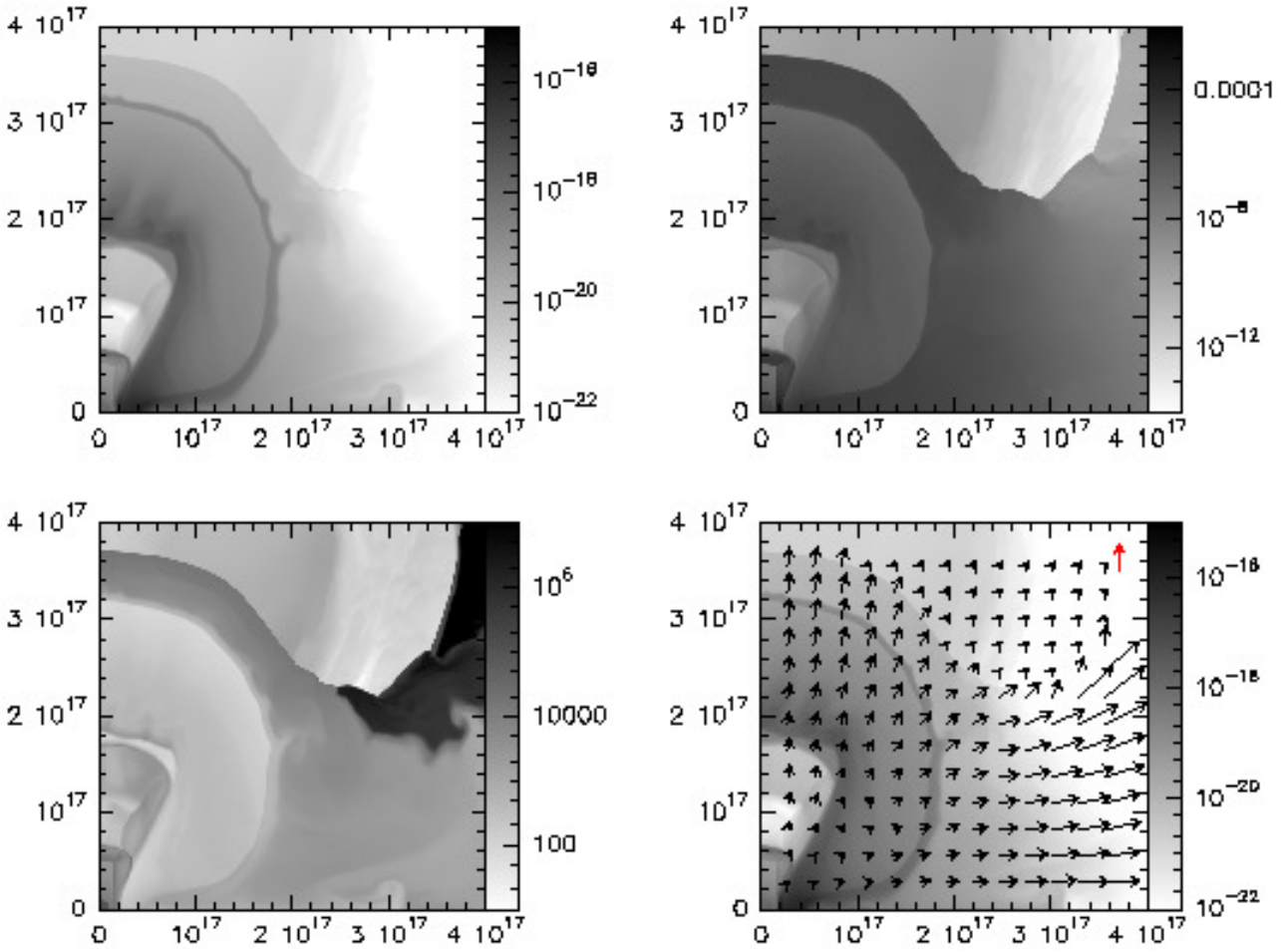

Fig. 3. Stratifications in one quadrant of density (*top left*), pressure (*top right*), temperature (*bottom left*), and velocity field superposed on the density map (*bottom right*) for Run A computed 120 yr after the major eruption of η Car. The vertical red arrow shown in the velocity-field stratification corresponds to 1000 km s^{-1}. The text gives a further description of the figure.

the nebula detected by Smith (2006), with a thin outer layer that traces the Homunculus shape and a thicker inner skin that resides in the interior of lobes just behind the thin outer shell. According to this author, this double-shell structure resembles a classic two-shock layer formed by the interaction of a wind with the ambient medium, which is consistent with the predictions of the numerical experiments presented in this work. On the other hand, the numerical simulations presented here show that Rayleigh-Taylor and Kelvin-Helmholtz instabilities are developed along the dense shell, as well as Richtemyer-Meshkov instabilities that are produced in the inner boundary of the thicker shell. These thermal instabilities in the dense shell may be related to the complex structure of the polar lobes.

Nevertheless, it is noteworthy that the numerical simulations presented here, in which an explosion, that lasted only a few years, interacts with a pre-outburst wind, that was ejected for a few decades, fail to reproduce the current physical size of the large Homunculus. Although the CSM interaction model proposed by Smith (2013) is able to match the light curve of the star 10−15 yr after the eruption, the predicted dynamical age of the polar lobes by the simulations (∼120 yr), when the physical extension of the polar lobes is $\pm 3.2 \times 10^{17}$ cm, is not consistent with the estimated value from observations (174 yr). On the other hand, the computed polar expansion velocity at this time is ≃800 km s^{-1}, which is somewhat higher than the observed value of ≃650 km s^{-1} of the Homunculus at high latitudes.

The numerical predictions presented in this work indicate that the outflow parameters proposed by Smith (2013), which fit his model, are not able to explain dynamical features of the present-day η Car nebula. It is noteworthy that the physical properties of the wind prior to the great eruption are not well constrained. A mass loss of 10 $M_\odot$ in the 30 yr pre-eruption phase assumed by this author does not seem supported by the light curve. That much mass loss in such a short time suggests that there would be some obscuration due to dust. At that time, the star was bright with an apparent magnitude $m_V \simeq 1$–2, while its normal state was $m_V \simeq 3$–4. Davidson (2012) deduced that η Car's effective temperature was $T_{\rm eff} \simeq 20\,000$–$25\,000$ K prior the eruption, and given the helium and nitrogen abundances of the Homunculus nebula, the star was probably a post-Main Sequence star in that epoch. Consequently, the stellar outflow properties were probably consistent with an evolved B-type supergiant wind, with a typical ejection velocity of a few hundred km s^{-1}, and a mass-loss rate of $\sim 10^{-4}$ $M_\odot$ yr^{-1}. Besides, the conditions of the post-outburst wind are not well restricted either. In this work, I have assumed similar outflow parameters to the present-day stellar wind, however, it is worth mentioning that η Car's wind parameters have changed since that epoch.

Mehner et al. (2010) present emission features in the spectrum of η Car that probably suggest a decrease in η Car's primary wind density. In other work, Davidson et al. (2015) show spectroscopic variations in the most recent periastron passages,

giving evidence of a progressive decline in the primary wind density. Furthermore, Humphreys et al. (2008) examined η Car's spectrum from 1892 to 1941, showing that high-excitation features, which are conspicuous today, were weak and perhaps absent throughout those years. The period from about 1900 to 1941 was one of relative quiescence for η Car, but a few years later its spectrum showed prominent high-excitation emission lines. These authors pointed out that η Car's rapid brightening during this time was probably due to dust destruction by UV radiation. All of these results give evidence that η Car's wind conditions have changed since the minor eruption ended, and it may be incorrect to assume a steady stellar wind, even though the post-eruption wind has no effect on the dynamics of the large Homunculus.

The physics involved in a giant eruption or supernova impostor event is an open issue in stellar astrophysics, and η Car's eruption in the 1840s represents the most notorious example of this sort of eruptive event. A giant eruption is a super-Eddington mass outflow, which is driven by continuum radiation pressure and can last months or years (see, for instance, Davidson 2016; Owocki & Shaviv 2012). In other work, the light echo spectra from η Car detected by Rest et al. (2012) provided important clues on the nature of η Car's giant eruption, leading to a debate about a steady stellar wind versus an explosion. Additionally, Owocki & Shaviv (2016), based on an updated analysis of the wind-outflow model using newer low-temperature opacity tabulations and accounting for the mass-loss implied by the $>10\ M_{\odot}$ mass now inferred for the large Homunculus, concluded that a low spectral temperature of ~5000 K is compatible with a wind model with the high mass loss inferred for the eruption. Nevertheless, such a cool spectra is not unique to a steady wind-outflow model but also to type II SN explosions. As pointed out by these authors, a key question is the timescale for variations in the outflow, and in the case of η Car's nineteenth century great eruption, the extended epoch for years is in favor of the steady wind scenario. Nevertheless, several arguments favoring the alternative scenario of an explosion have also been given. For instance, the study of the light echoes of η Car's giant eruption by Prieto et al. (2014) appears to be more consistent with the model of the great eruption as an explosion interacting with a strong pre-eruptive wind proposed by Smith (2013).

Finally, a comparison of the numerical simulations presented in this work for η Car's giant eruption as an explosion with those simulations carried out adopting an interacting-wind scenario (see, González et al. 2010) shows that the present predictions about the dynamical age of the large Homunculus nebula are not consistent with observations, which may suggest that the great eruption suffered by η Car in the middle of the nineteenth century was probably a super-Eddington wind rather than an explosion. Notwithstanding this, more realistic eruption models may be obtained from insights gleaned from both scenarios.

Acknowledgements. This research was supported by the UNAM-PAPIIT grant IN 112116. I thank A. C. Raga and P. F. Velázquez for their helpful comments on the numerical code. The author also thanks the useful comments and suggestions of the anonymous referee that improved the content and presentation of the paper.

References

Brouillette, M. 2002, Annu. Rev. Fluid Mech., 34, 445
Damineli, A. 1996, ApJ, 460, L49
Damineli, A., Conti, P. S., & Lopes. D. F. 1997, New Astron., 2, 107
Davidson, K. 2012 ASSL Eta Carinae and the Supernova impostors, 384, 43
Davidson, K. 2016, J. Phys. Conf. Ser., 728, Issue 2
Davidson, K., Smith, N., Gull, T. R., Ishibashi, K., & Hillier, D. J. 2001, AJ, 121, 1569
Davidson, K., Mehner, A., Humphreys, R. M., Martin, J. C., & Ishibashi, K. 2015, ApJ, 801, L15
Dwarkadas, V. V., & Balick, B. 1998, AJ, 116, 829
Dwarkadas, V. V., & Owocki 2002, ApJ, 581, 1337
Frank, A., Balick, B., & Davidson, K. 1995, ApJ, 441, L77
Frank, A., Ryu, D., & Davidson, K. 1998, ApJ, 500, 291
García-Segura, G., Langer, N., & Mac Low, M.-M. 1996, A&A, 305, 229
González, R. F., de Gouveia Dal Pino, E. M., Raga, A. C., & Velázquez, P. F. 2004a, ApJ, 600, L59
González, R. F., de Gouveia Dal Pino, E. M., Raga, A. C., & Velázquez, P. F. 2004b, ApJ, 616, 976
González, R. F., Villa, A. M., Gómez, G. C., et al. 2010, MNRAS, 402, 1141
Humphreys, R. M., Davidson, K., & Smith, N. 1999, PASP, 111, 1124
Humphreys, R. M., Davidson, K., & Koppelman, M. 2008, AJ, 135, 1249
Ishibashi, K., Gull, T. R., Davidson, K., et al. 2003, AJ, 125, 3222
Langer, N., García-Segura, G., & Mac Low, M.-M. 1999, ApJ, 520, L49
Maeder, A., & Desjacques, V. 2001, A&A, 372, L9
Mehner, A., Davidson, K., Humphreys, R. M., et al. 2010, ApJ, 717, L22
Morse, J. A., Davidson, K., Bally, J., et al. 1998, AJ, 116, 2443
Owocki. S. P., & Shaviv, N. J. 2012, ASSL Eta Carinae and the Supernova impostors, 384, 275
Owocki. S. P., & Shaviv, N. J. 2016, MNRAS, 462, 345
Portegies Zwart, S. F., & van den Heuvel, E. P. J. 2016, MNRAS, 456, 3401
Raga, A. C., Navarro-González, R., & Villagrán-Muniz, M. 2000, Rev. Mex. Astron. Astrofís., 36, 67
Rest, A., Prieto, J. L., Walborn, N. R., et al. 2012, Nature, 482, 375
Smith, N. 2005, MNRAS, 357, 1330
Smith, N. 2006, ApJ, 644, 1151
Smith, N. 2013, MNRAS, 429, 2366
Smith, N., Davidson, K., Gull, T. R., Ishibashi, K., & Hillier D. J. 2003, ApJ, 586, 432
Soker, N. 2001, MNRAS, 325, 584
Soker, N. 2004, ApJ, 612, 1060
Soker, N. 2007, ApJ, 661, 490
Steffen, W., Teodoro, M., Madura, T. I., et al. 2014, MNRAS, 442, 3316
Van Leer, B. 1982, ICASE Report No. 82
van Marle, A., Smith, N., Owoki, S. P., & van Veelen, B. 2010, MNRAS, 407, 2305
Vishniac, E. T. 1994, ApJ, 428, 186